Circuit modeling of multiband high-impedance surface absorbers in the microwave regime

Yashwanth R. Padooru,[1] Alexander B. Yakovlev,[1] Chandra S. R. Kaipa,[1] Francisco Medina,[2] and Francisco Mesa[3]
[1]*Department of Electrical Engineering, The University of Mississippi, University, Mississippi 38677, USA*
[2]*Department of Electronics and Electromagnetism, University of Seville, Seville 41012, Spain*
[3]*Department of Applied Physics 1, University of Seville, Seville 41012, Spain*
(Received 10 November 2010; revised manuscript received 5 March 2011; published 20 July 2011)

In this paper, we present a simple circuit model to study the absorption of electromagnetic waves by a multilayer structure with a high impedance surface in the microwave regime. The absorber consists of a stack of two-dimensional arrays of sub-wavelength meshes or patches separated by dielectric slabs and backed by a metallic ground plane, with a single resistive sheet placed on the top layer. We observe the appearance of low-frequency resonances of total absorption, which have been identified as the resonances of Fabry-Pérot type associated with the individual reactively loaded dielectric slabs (that are strongly coupled through the subwavelength grids). It is shown that these resonances lie within certain characteristic frequency band defined by the structural parameters of the absorber. The observed resonances are characterized by studying the electromagnetic field behavior using the circuit model and full-wave numerical program. In addition, we show that the patch array absorber provides stable resonances with respect to the angle and the polarization of obliquely incident plane waves.

DOI: 10.1103/PhysRevB.84.035108 PACS number(s): 78.20.Ci, 41.20.−q, 42.25.Bs

I. INTRODUCTION

Since the invention of the classical Jaumann and Salisbury absorbing structures (see, for a detailed historical review, the book on frequency selective surfaces by Munk[1]), there have been various absorbers invented, new concepts formalized, and advanced design procedures added to the existing ones. Even nowadays, there is a growing interest in the study of these structures, mainly in the physics community, due to their wide range of applications in the electromagnetic spectrum from microwave to optical frequencies.

In recent years, there has been considerable interest in the enhancement of the performance of absorbers using metamaterials[2–9] because of their peculiar properties, which are not available in conventional materials. In Ref. 2, it was shown that by using resonant elements (electric ring resonator backed by a cut wire) in the unit cell, absorption of nearly unity can be achieved at microwave frequencies. In that paper, the absorption is obtained by the appropriate choice of effective permittivity and effective permeability, such that the impedance of the absorber is matched to free space.[2] Based on this idea, other possibilities have been put forward to extend the designs to higher frequencies[3–8] and for large incidence angles.[3,5,7,8] Also, electrically thin absorbers based on high-impedance surfaces (HIS's)[10–13] have been introduced in the microwave regime. Following Ref. 10, an absorption resonance is achieved by combining the properties of the HIS with the absorption of a resistive sheet. In practice, the resistive sheet can be realized using commercially available resistive materials placed on the HIS[11] or with surface-mounted resistive elements interconnecting the metallic parts of two-dimensional subwavelength elements.[12,13] More recently, ultrathin absorbers have been introduced, with losses either in the dielectric slab[14] or in the metallic elements of frequency-selective surfaces.[15,16]

The common feature of all of the aforementioned absorbing structures is that they operate in a single narrow frequency band with high absorption at a specific frequency (independently of their specific operating frequency regimes). This fact limits their use in applications such as spectroscopic detection and identification of explosives, contaminations, and rare-earth ions, which have distinct absorption features at multiple frequencies.[17,18] To overcome these shortcomings, dual-band metamaterial absorbers[19,20] have been proposed. In these designs, the unit cells of the two single-band resonators were combined together to form a single unit cell with dual-band resonances. Although these absorbers show good absorptivity at dual frequencies, they operate only at the normal incidence of the impinging electromagnetic wave. Hence, wide-angle and polarization-insensitive multiband absorbers with two or more absorption peaks are highly desirable.

In this work, we will use the idea of a single-band HIS absorber[10] adapted to a layered environment (with the geometry of a typical configuration shown in Fig. 1), and demonstrate that this structure [formed by a stack of two-dimensional (2D) subwavelength grid elements] exhibits multiple absorption peaks in the microwave regime. It is important to note that the absorption characteristics that we investigate here are quite different from those described in Refs. 19 and 20, wherein the absorption resonances depend directly on the resonances of the unit-cell resonators. In order to achieve these multiple absorption peaks, the resonators in Refs. 19 and 20 had multiple resonant elements in the unit cell, which led to complex designs of the unit-cell geometry. In contrast, we explore here a completely different physical effect not directly related to the resonances of the unit-cell elements. Based on a circuit theory model, we demonstrate that the absorption resonances are of Fabry-Pérot (FP) type associated with the individual reactively loaded dielectric slabs that are strongly coupled through the sub wavelength grid or patch elements.

Circuit models have been used for a long time in the context of electrical engineering with remarkable success. For instance, the problem of propagation of electromagnetic waves through wire media, which has been essential for the development of metamaterial science (wire media behave as plasma with negative index of refraction at optical frequencies), was addressed several decades ago by using circuit analogies.[21,22] More recently, circuit models for analyzing HIS

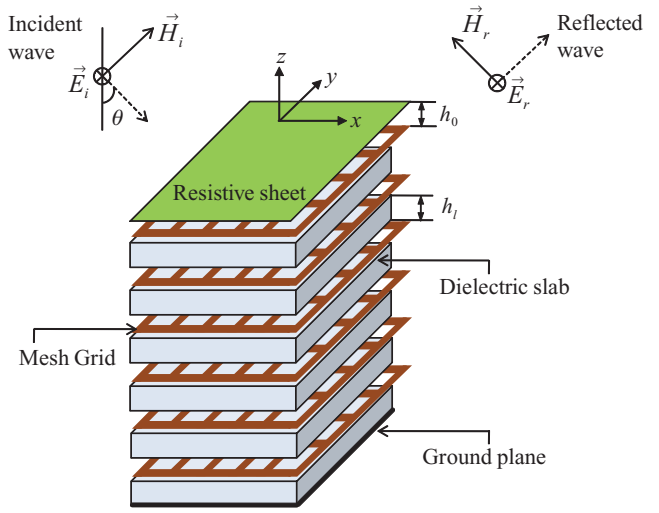

FIG. 1. (Color online) Exploded schematic of the multilayer HIS absorber formed by mesh grids of subwavelength dimensions.

absorbers[14,16,23,24] have been proposed with the aim of avoiding the lengthy and cumbersome computations demanded by the numerical simulations. Indeed, problems closely related to the ones treated in this work have been analyzed following the circuit approach presented in Refs. 25–27. Also, it should be mentioned that the circuit modeling can be used at optical frequencies,[28] with the functionality of inductors, capacitors, and resistors realized using plasmonic and nonplasmonic nanoparticles. Apparently, this strategy, which is well known to microwave and antenna engineers, has not spread enough among the optics community. Furthermore, since circuit models do not provide exact solutions, they have to be thoroughly validated in each new application, which motivates the study carried out in this work.

Thus, and due to the ease of implementation and direct connection with the physics of the problem, we explore the advantages of the circuit model to explain the absorptivity in multilayer HIS absorbers. The method of analysis is based on the circuit theory model of the stacked subwavelength grids,[27] wherein the analytical expressions for the grid impedances (admittances) are obtained in terms of the effective circuit parameters from the full-wave scattering problem.[29,30] In this paper, we add lumped resistors or a single resistive sheet on the top layer of a stack of grid or patch arrays, and study the absorption mechanisms of the entire multilayer structure. Due to a small electrical size of the unit cell, the grid provides a mechanism for the excitation of higher-order evanescent fields, which spread over a certain distance around the grid. However, if the distance between the adjacent grids is large enough (typically larger than the period of the unit cell), the higher-order mode interactions can be neglected, and the grids interact primarily through the single transverse electromagnetic (TEM) mode. In such a situation, the circuit model gives fairly accurate results, as described in Ref. 27.

In particular, we concentrate on the case of a two-layer HIS formed by mesh grids without and with the resistive sheet, and relate the physical mechanisms of HIS and absorption resonances to the transmission resonances observed in a four-layer structure (without the ground plane) formed by the same mesh grids.[27] Even though the considered configuration is electrically thick when compared to the operating wavelength (greater than a quarter-wavelength in dielectric), we employ this example due to the similarities in the structure and the resonances studied in Ref. 27. In that paper, it was demonstrated that the transmission spectra for each transmission band have a number of peaks (as FP resonances) equal to the number of FP cavities (formed by reactively loaded dielectric slabs). In a similar way, we show now that the multilayer mesh or patch grid absorbers exhibit the same kind of FP-like resonances. It is observed that the resonances of total absorption lie within a characteristic frequency band defined by the lower and upper band edges. These edge frequencies correspond to the first and the last resonance modes, and a comprehensive study of the electromagnetic field distribution associated with these resonances is provided using the circuit model and full-wave commercial solver HFSS.[31] Also, it is observed that the HIS absorber formed by mesh grids is sensitive to the angle and the polarization of the impinging plane waves. In order to overcome this problem, we present a multilayer HIS absorber formed by the patch arrays, with stable resonances for different incident angles and polarizations. In addition, we demonstrate that if a tunable resistive sheet with a wide range of admittance values is chosen, the multilayer patch array absorber is capable of absorbing the plane waves for large incident angles at multiple frequencies.

The paper is organized as follows. In Sec. II, the formalism of the circuit model for the analysis of the multilayer HIS absorbers is presented. Section III focuses on the study of the HIS absorbers formed by mesh grids. The observed resonances are related to the FP resonances of the series of coupled individual cavities through the resonant field behavior. The results of the HIS absorbers formed by patch arrays are discussed in Sec. IV. The conclusions are drawn in Sec. V.

II. CIRCUIT MODEL ANALYSIS

Consider a plane wave incident on the multilayer HIS absorber as shown in Fig. 1. It is assumed that each dielectric layer is homogeneous and isotropic of thickness h_l, and characterized with relative permittivity ε_l, $l = 1,2,\ldots,m$ and permeability of free space. Provided that for the frequencies of interest the interaction between the grids takes place through

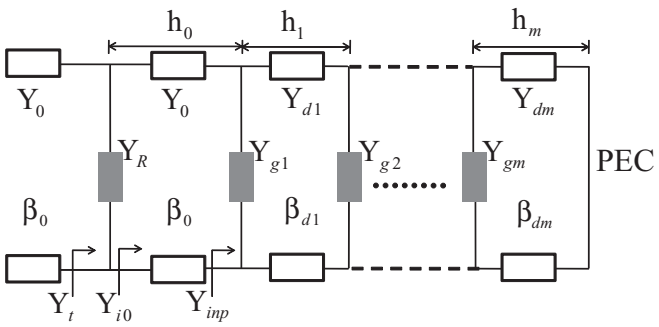

FIG. 2. Transmission-line network for the multilayer structure with subwavelength periodic elements; Y_0,β_0 are the characteristic admittance and propagation constant of the air filled region; Y_{dl} and β_{dl} are the same parameters for the corresponding dielectric filled regions.

a single TEM mode, the circuit model shown in Fig. 2 gives an appropriate description of the system in Fig. 1. The shunt reactances $Y_{g1}, Y_{g2}, \ldots, Y_{gm}$ (grid admittances) account for the below-cutoff evanescent higher-order modes scattered by the metal grids in each layer. The lossy resistive sheet represented by an admittance Y_R, in parallel with the grid admittance Y_{g1}, is placed at a distance h_0 from the multilayer structure. The medium between the resistive sheet and the multilayer structure is assumed to be free space. In practice, the distance h_0 is either zero or electrically small (which leaves an air gap). The parameters of the transmission line in Fig. 2, propagation constants β_0 for the air filled section and β_{dl} for the dielectric filled sections, and the corresponding characteristic admittances Y_0 and Y_{dl} are known in closed form. The expressions for these parameters for transverse electric (TE) and transverse magnetic (TM) polarizations are

$$\beta_0 = \frac{\omega}{c}, \quad \beta_{dl} = \beta_0\sqrt{\varepsilon_l - \sin^2\theta}, \tag{1}$$

$$Y_0^{\mathrm{TE}} = Y_0\cos\theta, \quad Y_0^{\mathrm{TM}} = \frac{Y_0}{\cos\theta}, \tag{2}$$

$$Y_{dl}^{\mathrm{TE}} = Y_0\sqrt{\varepsilon_l - \sin^2\theta}, \quad Y_{dl}^{\mathrm{TM}} = \frac{Y_0\,\varepsilon_l}{\sqrt{\varepsilon_l - \sin^2\theta}}, \tag{3}$$

where $Y_0 = \sqrt{\varepsilon_0/\mu_0} \approx 1/377$ S is the intrinsic admittance of free space, θ is the incidence angle, ω is the angular frequency, and c is the speed of light in vacuum. Since the size of the unit cell considered in this work is electrically small, accurate estimations for the grid admittances based on the dynamic solution for some periodic structures (patch arrays, mesh grids, among others) are available in the literature. Following Ref. 30, the mesh or patch grid behaves mainly as an inductive or capacitive load, and the analytical expressions for grid admittance Y_{gl} for TE and TM polarizations can be obtained as follows:

$$Y_{gl}^{\mathrm{TE}} = \frac{1}{j\omega L_{gl}^{\mathrm{TE}}}, \quad L_{gl}^{\mathrm{TE}} = \frac{\eta_0 D}{2c\pi}\ln\left[\csc\left(\frac{\pi w}{2D}\right)\right], \tag{4}$$

$$Y_{gl}^{\mathrm{TM}} = \frac{1}{j\omega L_{gl}^{\mathrm{TM}}}, \quad L_{gl}^{\mathrm{TM}} = \frac{\eta_0 D}{2c\pi}\ln\left[\csc\left(\frac{\pi w}{2D}\right)\right]\left(1 - \frac{\sin^2\theta}{2\varepsilon_l^{qs}}\right), \tag{5}$$

$$Y_{gl}^{\mathrm{TE}} = j\omega C_{gl}^{\mathrm{TE}}, \quad C_{gl}^{\mathrm{TE}} = \frac{2D\varepsilon_l^{qs}}{c\eta_0\pi}\ln\left[\csc\left(\frac{\pi w}{2D}\right)\right]\left(1 - \frac{\sin^2\theta}{2\varepsilon_l^{qs}}\right), \tag{6}$$

$$Y_{gl}^{\mathrm{TM}} = j\omega C_{gl}^{\mathrm{TM}}, \quad C_{gl}^{\mathrm{TM}} = \frac{2D\varepsilon_l^{qs}}{c\eta_0\pi}\ln\left[\csc\left(\frac{\pi w}{2D}\right)\right], \tag{7}$$

where csc stands for the cosecant function, $\eta_0 = \sqrt{\mu_0/\varepsilon_0} \approx 377\ \Omega$ is the intrinsic impedance of free space, $\varepsilon_l^{qs} = (\varepsilon_l + \varepsilon_{l+1})/2$ is for interior grids ($l = 2,3,\ldots,m-1$), and $\varepsilon_l^{qs} = (\varepsilon_l + 1)/2$ is for the grid located at the upper interface ($l = 1$). The geometrical parameters D and w of the inductive and capacitive grid are defined in Fig. 3(b) and Fig. 12(b) in the sections to follow.

It is well known that for a HIS structure[32,33] (single-band or multiband) at resonance, the surface admittance is zero, resulting in a zero reflection phase. In Fig. 2, Y_{inp} corresponds to the input admittance of the HIS structure. Hence, at resonance Y_{inp} is zero and the admittance of the open-circuit termination of the air-gap section (for small h_0) is given by

$$Y_{i0} = \mathrm{j}Y_0\tan\beta_0 h_0 \approx 0\,. \tag{8}$$

Thus, the total surface admittance Y_t of the HIS absorber is equal to admittance of the resistive sheet Y_R. If Y_R is chosen in such a way that $Y_R = Y_0^{\mathrm{TE,TM}}$ [$Y_0^{\mathrm{TE,TM}}$ are given in Eq. (2)], then the admittance of the structure is matched to the intrinsic admittance of free space. Under this condition, the incident field is absorbed by the structure and we have reflection nulls ($S_{11} = 0$) or absorption peaks ($\mathcal{A} = 1 - S_{11}^2$). Since the system is backed by a perfect electric conductor (PEC), no transmission is possible ($S_{12} = 0$) and thus the total incident energy is absorbed by the resistive sheet and dissipated as heat. In practice, dielectric slabs and metal grids have small losses and absorb a fraction of the incident energy.

In general, the formalism of the circuit model presented here can be directly applied to the analysis of wide-band absorption properties of multilayer structures with dielectric slabs of different thicknesses and permittivities, and arbitrary subwavelength resistive grids (e.g., patch arrays, Jerusalem cross arrays, and others) with the analytical expressions for the grid admittance or impedance available in the literature.[30,34] However, in this paper we focus our attention on the study of FP-type resonances in multilayer structures with identical grids and identical dielectric slabs.

III. MESH GRID ABSORBERS

In this section, the absorption properties of the multilayer HIS absorbers formed by mesh grids are analyzed using the circuit model formalism given in Sec. II. Specifically, we study the two-layer mesh grid absorber in order to explain the physical mechanisms of the resonances based on the resonant field behavior using the circuit model and numerical solutions. The resonances corresponding to the lower and upper frequency band edges of the absorption band in a multilayer configuration are explained in terms of the finite number of strongly coupled FP cavities.

A. Two-layer mesh grid absorber

The absorber (shown in Fig. 3) is composed of two identical mesh grids printed on two identical dielectric slabs, with a resistive sheet placed on the top and a PEC ground plane at the bottom. Each mesh grid has the period $D = 5$ mm and strip width $w = 0.15$ mm, and each dielectric slab is of thickness $h = 6.35$ mm with relative permittivity $\varepsilon = 3$. The admittance of the resistive sheet Y_R is chosen to be approximately $1/377$ S (for the normal plane-wave incidence). Since for the frequencies of interest (1–20 GHz) the period of the unit cell D is meaningfully smaller than λ_0 and the separation between the successive grids $h > D$ (higher-order interactions are negligible), the simple circuit model shown in Fig. 2 is appropriate for our analysis purposes. Consider the structure shown in Fig. 3 without the resistive sheet, and assume that it acts as a HIS at resonance ($Y_{\mathrm{inp}} = 0$), reflecting the incident field with zero reflection phase. Since the HIS is impenetrable, in the absence of losses its reflectance is equal to unity. The circuit model results (termed "Analytical" in the figures) for the reflection phase characteristics of the HIS structure are shown

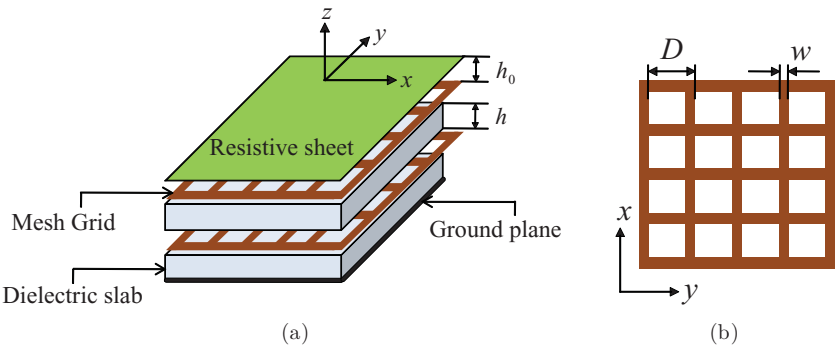

FIG. 3. (Color online) (a) Exploded schematic of the two-layer mesh grid separated by dielectric slabs, with a resistive sheet placed on the top and a PEC ground plane at the bottom. (b) Top view of the mesh grid.

in Fig. 4 for the case of normal incidence. These results show a very good agreement with the HFSS results also shown in the figure. Since the lattice in this work is square, the mesh grid (as well as the patch grid) is symmetric under rotation of 90° and, therefore, the effective grid admittance (understood in the sense of homogenization) is the same for normal incidence for both TE and TM polarizations, independent of the polarization angle. In Fig. 4, it can be observed that the structure has two resonances at 7.917 and 12.16 GHz corresponding to the zero reflection phase, labeled as A and B. It is interesting to note that the HIS structure is equivalent to the antisymmetric excitation (associated with placing a PEC wall in the middle) of the geometry analyzed in Ref. 27. Thus, following Ref. 27, we have two FP cavities that are strongly coupled through the square holes of each grid, i.e., two reactively loaded dielectric slabs. Also, the observed resonances A and B have the same physical nature as the resonances B and D in the four-layer structure formed with five identical mesh grids in Ref. 27 with the resonance frequencies of 8.06 and 12.2 GHz, respectively. Now, consider a resistive sheet ($Y_R \approx 1/377$ S) placed in close proximity to the HIS structure. The distance h_0 is assumed to be small (an air gap of 0.1 mm thickness is used) so that the effect of the air gap can be neglected. In such a case, the structure still retains the same FP-like resonances A and B, however there is no reflection because of the perfect match of the surface admittance (Y_t in Fig. 2) of the absorber to free space. Figure 5 shows the predictions of the analytical model for the case of normal incidence. It is seen that the results of the circuit model are again in good agreement with the HFSS results. It is worth pointing out that, in the two-layer HIS absorber and the one studied in Ref. 27, the corresponding resonances of absorption and transmission are associated with the perfect match of the surface admittance to the intrinsic admittance of free space. Hence, it is important to verify the field distributions at the resonance frequencies, and at the same time compare the predictions of the circuit model with HFSS.

The electric-field distributions based on the results of the circuit model and HFSS, corresponding to the two resonance modes (A and B) of the absorption band, are shown in Fig. 6. Circuit model results are in good agreement with the numerical results, which shows that our model captures the electromagnetic details of the structure. For the field distributions corresponding to the first resonance (mode A), there is no low value of the electric field near and over the internal grid, and also the fields in the dielectric layers are in phase with each other. By contrast, for the second resonance (mode B), the field value is relatively low over the internal grid, and the fields in the dielectric layers are out of phase. Also, the observed field distributions in Fig. 6 have the same qualitative behavior as the fields in the first two layers (modes B and D) in Ref. 27. However, in Ref. 27, the dominant TEM mode is transmitted through the structure for the modes B and

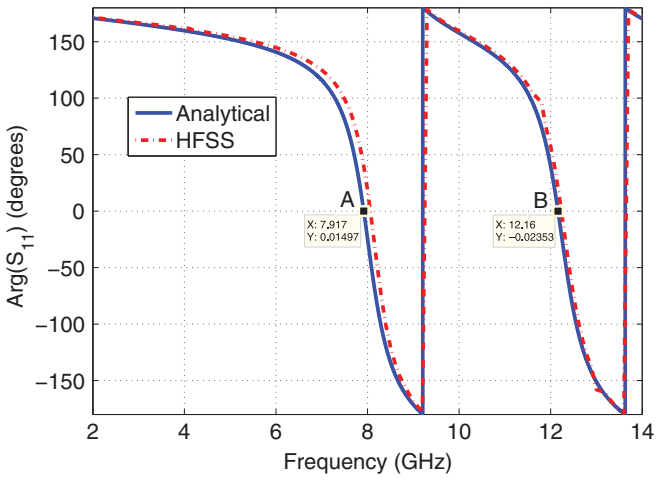

FIG. 4. (Color online) Reflection phase behavior of the two-layer mesh structure in the absence of resistive sheet, calculated using the circuit model and HFSS.

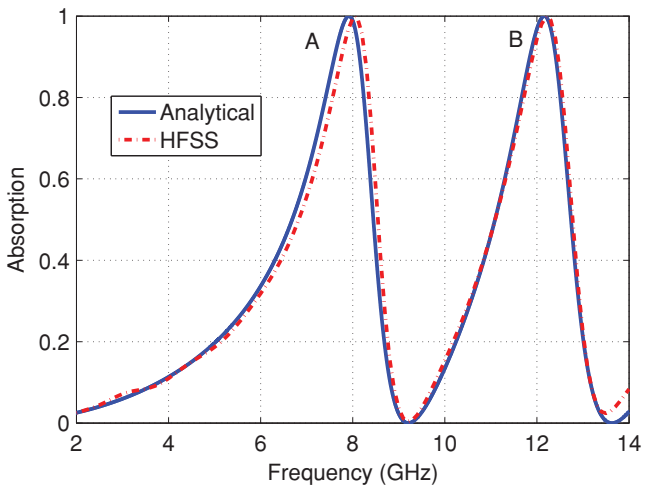

FIG. 5. (Color online) Absorptivity of the two-layer HIS absorber as a function of frequency, calculated with the circuit model and HFSS.

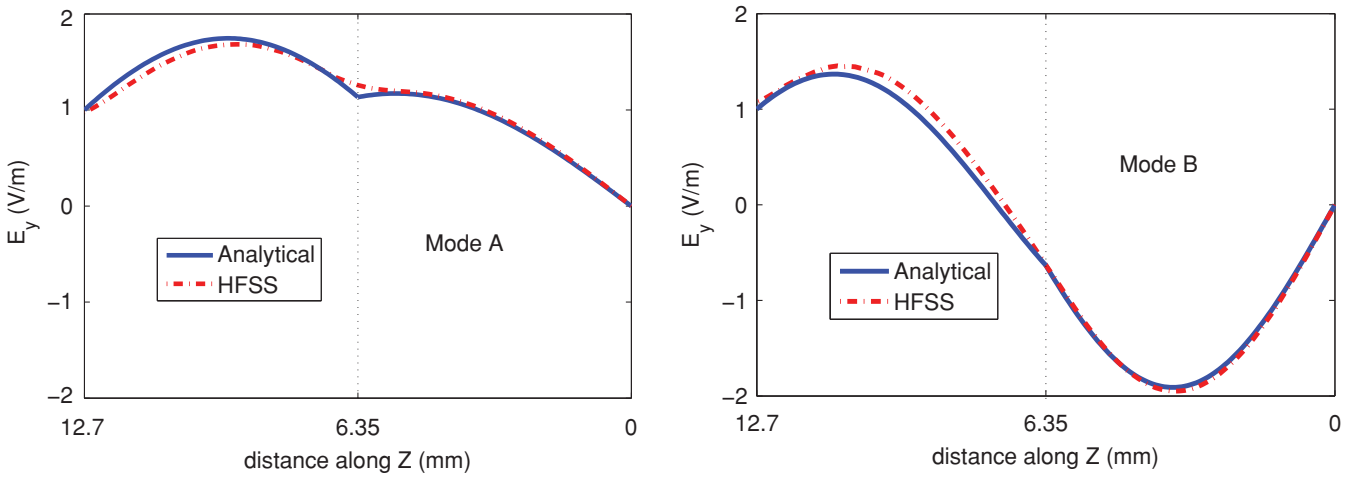

FIG. 6. (Color online) Comparison of the analytical and HFSS results of the electric-field distributions in the two-layer HIS mesh grid absorber for (a) mode A and (b) mode B. HFSS results are obtained by calculating the field along a line in the z direction through the center of the holes.

D (which correspond to transmission peaks), and in the case of a two-layer absorber it is absorbed by the resistive sheet for the modes A and B (absorption peaks).

To understand the physics of absorption in the two-layer HIS absorber (shown in Fig. 3), in Fig. 7 we compare the total electric-field distributions of the HIS structure, with and without the resistive sheet at normal incidence, for the resonant modes using the circuit model and HFSS. The fields are calculated inside the cavities and in the air regions to explain how these structures interact with the incident plane wave [with the electric field of magnitude 1 V/m peak-to-peak (p-p)]. The first observation that can be drawn from Fig. 7 is that the field distributions predicted by the circuit model agree well with HFSS. Slight disagreements are expected around the grid positions, because the analytical model calculates the "macroscopic" field (average field over the period), and the HFSS provides the "microscopic" field (near field at each point) of the transverse electromagnetic waves. However, the microscopic and macroscopic fields are comparable for the subwavelength mesh grids.[27] The position of the mesh grids is shown by the vertical dotted lines. It can be observed that the field values for the two modes are meaningfully larger in the absence of the resistive sheet, as expected. This is because at resonance, the HIS reflects the field with zero reflection phase ($S_{11} = +1$), and the total electric field is equal to twice the incident field (note that $E_y = 2$ V/m at $z = 12.7$ mm). However, in the presence of the resistive sheet, the reflected field is absorbed and dissipated as heat, and the total electric field is equal to the incident field (in the air region). It should be noted that for the HIS structure with and without the resistive

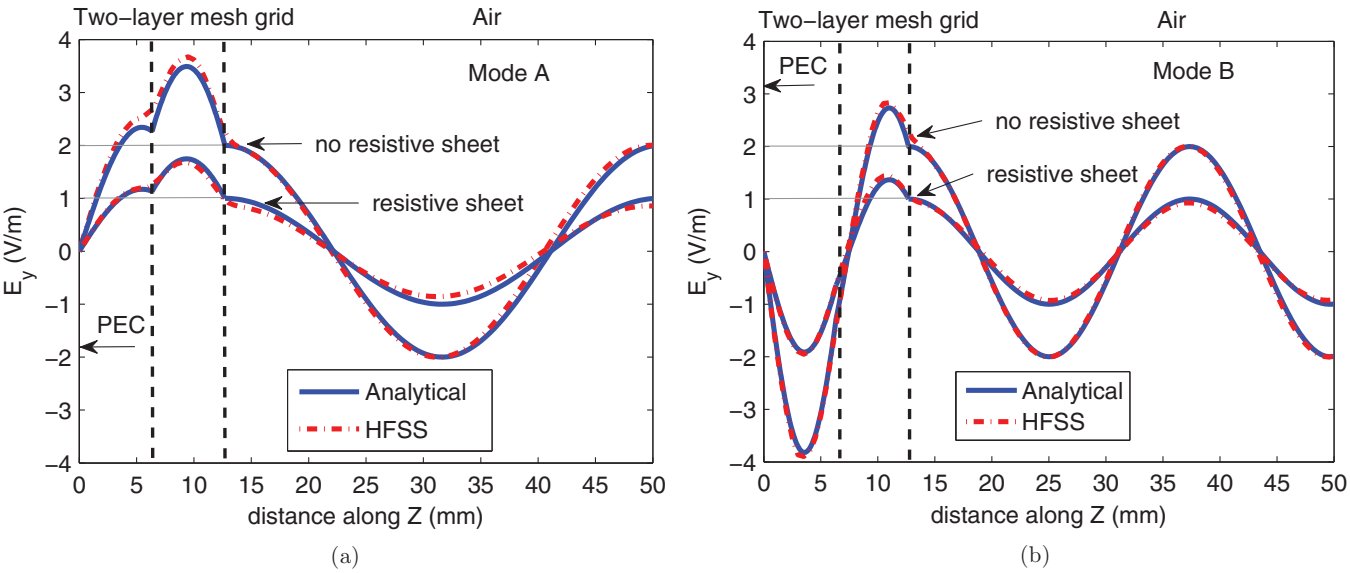

FIG. 7. (Color online) Total electric-field distributions of the two-layer mesh grid structure with and without the resistive sheet for (a) mode A and (b) mode B. The dotted vertical lines denote the position of the mesh grids.

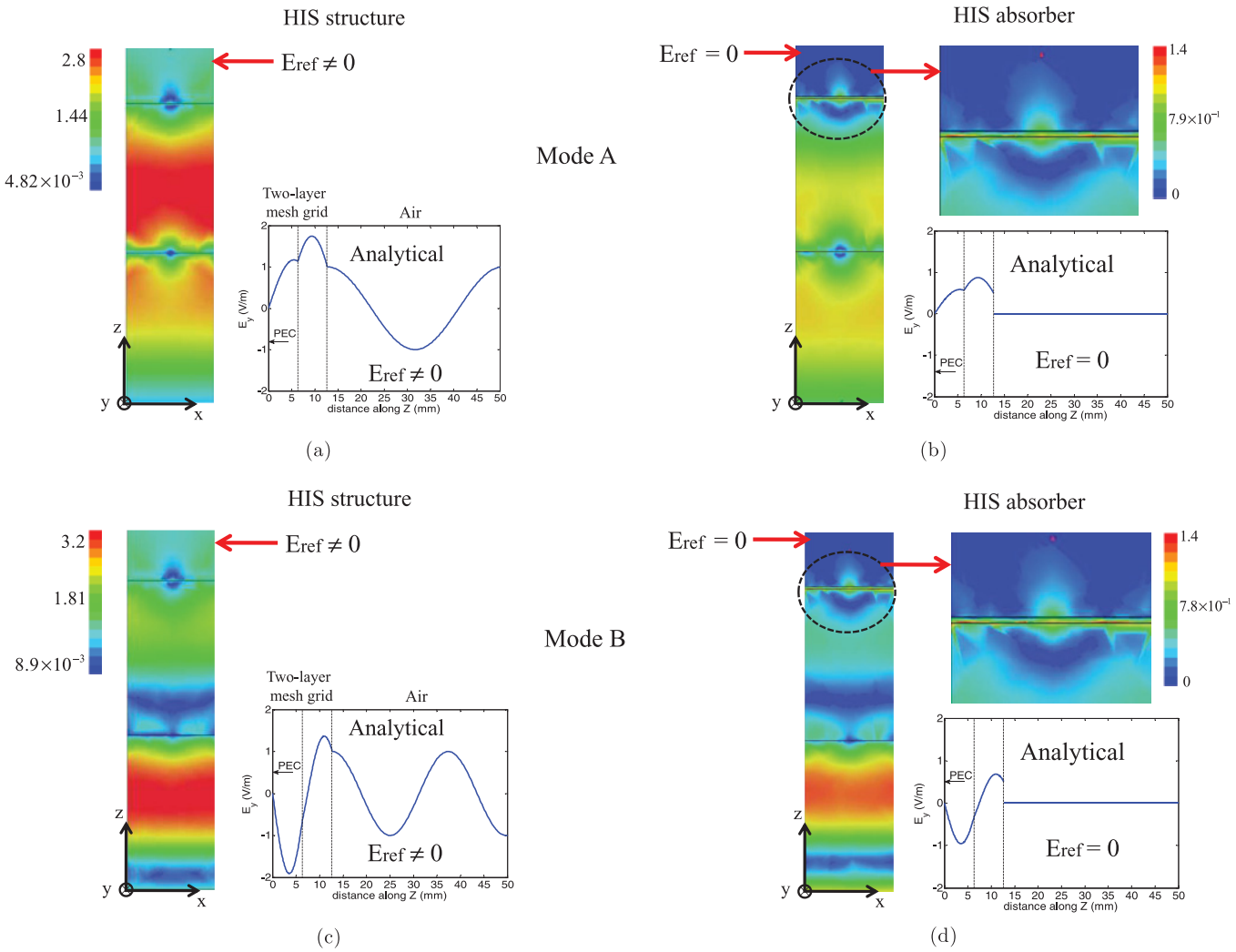

FIG. 8. (Color online) Reflected electric-field distributions of the two-layer mesh grid structure: (a) mode *A* without the resistive sheet, (b) mode *A* with the resistive sheet, (c) mode *B* without the resistive sheet, and (d) mode *B* with the resistive sheet.

sheet, the fields (incident and reflected) inside the cavities add in phase. Next we study the behavior of the reflected electric field for the modes *A* and *B* of the HIS structure (without the resistive sheet) and the absorber (with the resistive sheet). The full-wave simulation results are shown in Fig. 8 for the case of normal incidence. In the absence of the resistive sheet, it can be observed from Figs. 8(a) and 8(c) that the reflected field for the resonance modes *A* and *B* is quite significant in the air region. As expected, a region of zero field is observed in the air region in the presence of the resistive sheet, as shown in Figs. 8(b) and 8(d). Since there is no reflected field in the air region, the fields are trapped inside the structure. With the resistive sheet being the only lossy part in the system, it completely absorbs the total (incident and reflected) field. This is shown in Figs. 8(b) and 8(d) (magnified panels), where a strong concentration of the fields in the region close to the resistive sheet is observed.

In order to further validate this point, we calculate the surface loss density of the resistive sheet for the two resonance modes using full-wave simulations, shown in Fig. 9. Due to the finite resistivity of the sheet, the surface currents induce resistive losses in the sheet, resulting in the power dissipated as heat.

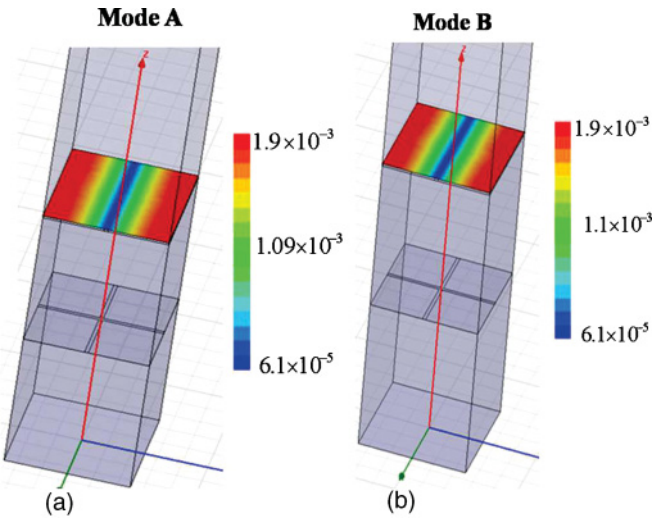

FIG. 9. (Color online) Simulation results of the surface loss density of the two-layer mesh grid HIS absorber, calculated using HFSS for (a) mode *A* and (b) mode *B*.

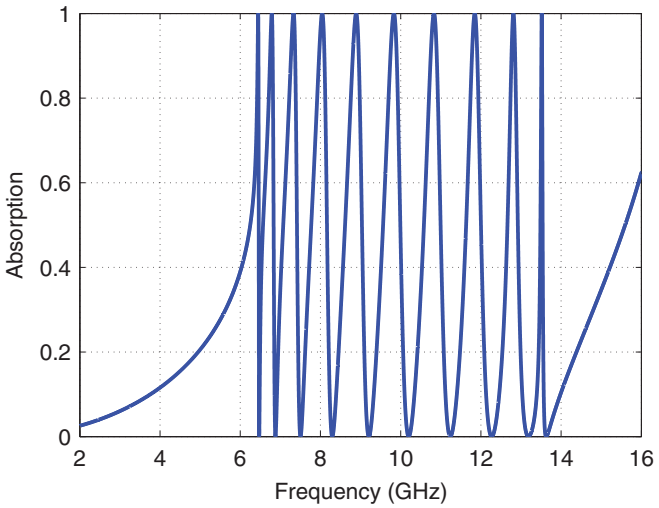

FIG. 10. (Color online) Analytical results of the absorption in the ten-layer HIS mesh grid absorber at normal incidence.

B. Multilayer mesh grid absorber

In the previous example, it has been shown that the two-layer HIS absorber exhibits two FP-like resonances of complete absorption corresponding to the two FP cavities. It is then convenient to study the characteristics of the absorption band and its dependence on the structural parameters. For this purpose, we apply the circuit model to study the absorption characteristics in structures formed by a large number of identical layers (mesh grids and dielectric slabs). We consider the field distributions corresponding to the first and the last resonance frequencies since the frequencies related to the lower and upper band edges define the absorption band. It should be noted that nonidentical dielectric slabs (with a proper choice of permittivity and thickness) can be used in order to achieve the wide-band, band-pass, and band-stop absorption characteristics. These types of structures have potential applications as multiband absorbers and filters, although their study is beyond the scope of the present work. Figure 10 shows the absorption characteristics of a ten-layer absorber and all the peaks are within the characteristic frequency band. The absorber is formed by a stack of ten identical mesh grids printed on ten identical dielectric slabs (with the same geometrical dimensions used in the previous example) with a resistive sheet placed on the top and with the last dielectric slab backed by a PEC ground plane. In Fig. 10, it can be observed that there are ten peaks (resonances) of absorption (corresponding to the ten FP cavities), with all the peaks within the characteristic frequency band. It should be noted that, with an increase in the number of identical layers, the number of absorption peaks is equal to the number of dielectric slabs. Also, there are no significant changes in the frequencies corresponding to the lower and the upper resonances of the absorption band with a large number of layers. The frequencies corresponding to the first (f_{LB}) and the last (f_{UB}) resonances for a different number of layers are given in Table I. The field distributions corresponding to the lower and upper frequency band edges of a ten-layer structure are shown in Fig. 11. Interestingly, the field distributions corresponding to the first and the last resonances are of the same qualitative behavior of the two-layer structure (modes *A* and *B*, as shown in Fig. 6), irrespective of the number of layers. For the field distribution corresponding to the first

TABLE I. Frequencies of the lower and upper band edges with respect to the number of layers.

No. of layers	f_{LB} (GHz)	f_{UB} (GHz)
2	7.917	12.16
5	6.713	13.25
10	6.447	13.52
20	6.363	13.60
30	6.347	13.62

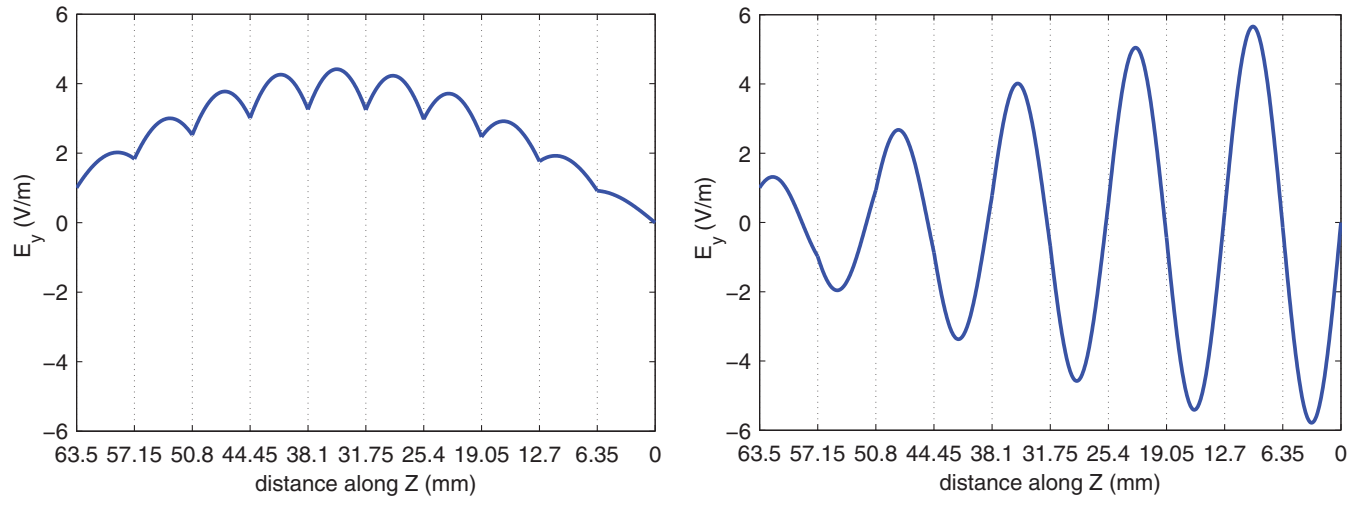

FIG. 11. (Color online) Analytical results of the field distributions in the ten-layer HIS mesh grid absorber for (a) first resonance mode and (b) last resonance mode.

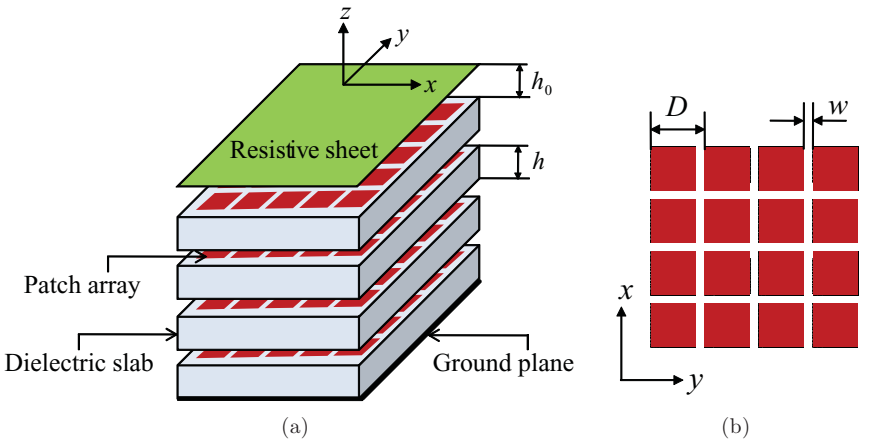

FIG. 12. (Color online) Exploded schematic of the multilayer patch array HIS absorber. (a) 3D view and (b) top view showing the unit-cell dimensions of the patch array.

resonance, the fields in the successive layers are in phase, and there is a significant contribution from the grids. This means that the frequency corresponding to the lower band edge is dependent on the dimensions of the mesh grid. However, for the field distribution corresponding to the last resonance, the fields in the adjacent layers oscillate out of phase, with no significant contribution from the mesh grids. The frequency corresponding to the upper band edge is equal to the FP condition[35] (half-wavelength) of a single dielectric layer,[27] and is largely independent of the grid. It should be noted that a similar type of field behavior has been observed in Ref. 27, where the analytical expressions for the lower and upper transmission peaks based on the analysis of an infinite structure have been presented.

IV. PATCH ARRAY ABSORBER

A. Normal incidence

Here we consider a multilayer HIS patch absorber as shown in Fig. 12. The structure is formed with identical patch arrays separated by dielectric slabs on a PEC ground plane, with a resistive sheet placed on the top. The analysis is carried out using the circuit model formalism given in Sec. II, with the appropriate grid admittance for the patch array given by Eqs. (6) and (7) for TE and TM polarizations, respectively. In the previous section, it has been shown that the multilayer mesh grid absorbers exhibit multiple FP-like resonances that lie within a characteristic frequency band. A similar phenomenon is observed in the present case of a multilayer HIS patch absorber, with the fields in the dielectric layers coupled through the capacitive grids.

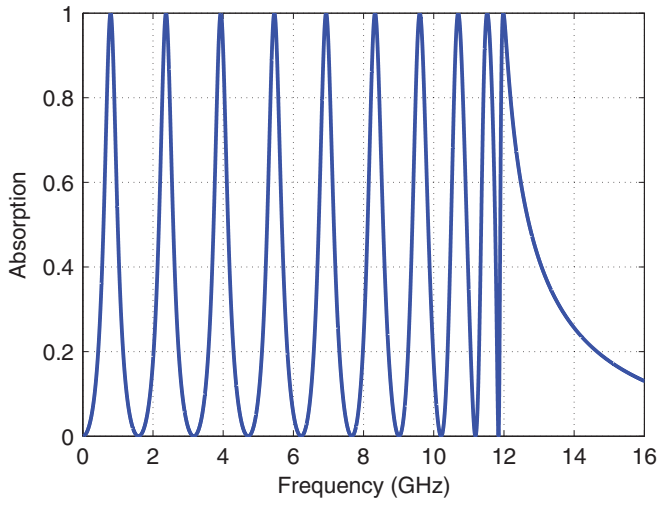

FIG. 13. (Color online) Analytical results of the absorption peaks in a ten-layer HIS patch absorber at normal incidence.

Figure 13 shows the analytical results of the absorption characteristics for a ten-layer HIS patch grid absorber formed by ten identical patch grids printed on the corresponding dielectric layers. Each patch array has the period $D = 2$ mm and the gap $w = 0.2$ mm, and each dielectric slab is of thickness $h = 2$ mm with relative permittivity 10.2. The admittance of the resistive sheet is chosen to be $1/377$ S for normal incidence. It can be observed that there are ten peaks of complete absorption corresponding to the ten layers (cavities) in the system. The resonance frequencies corresponding to the lower and the upper band edge for a different number of layers are given in Table II. The table shows that with an increase in the number of layers, the lower band-edge frequency decreases and the upper band-edge frequency remains almost the same. It should be noted that if an infinite number of layers is considered along the z direction (as was done in Ref. 27) and the resulting periodic structure is analyzed, then the mesh-loaded slabs behave as a pass-band structure while the patch-loaded slabs behave as a low-pass filter. This is the reason why the first resonance in the patch-loaded structure tends to zero frequency as the number of layers is increased. It is also possible to achieve higher-order pass bands for the patch-loaded periodic structure. An interesting practical

TABLE II. The lower and upper band-edge frequencies with respect to the number of layers.

No. of layers	f_{LB} (GHz)	f_{UB} (GHz)
2	3.89	10.56
5	1.57	11.77
10	0.79	11.98
25	0.32	12.06
30	0.26	12.06

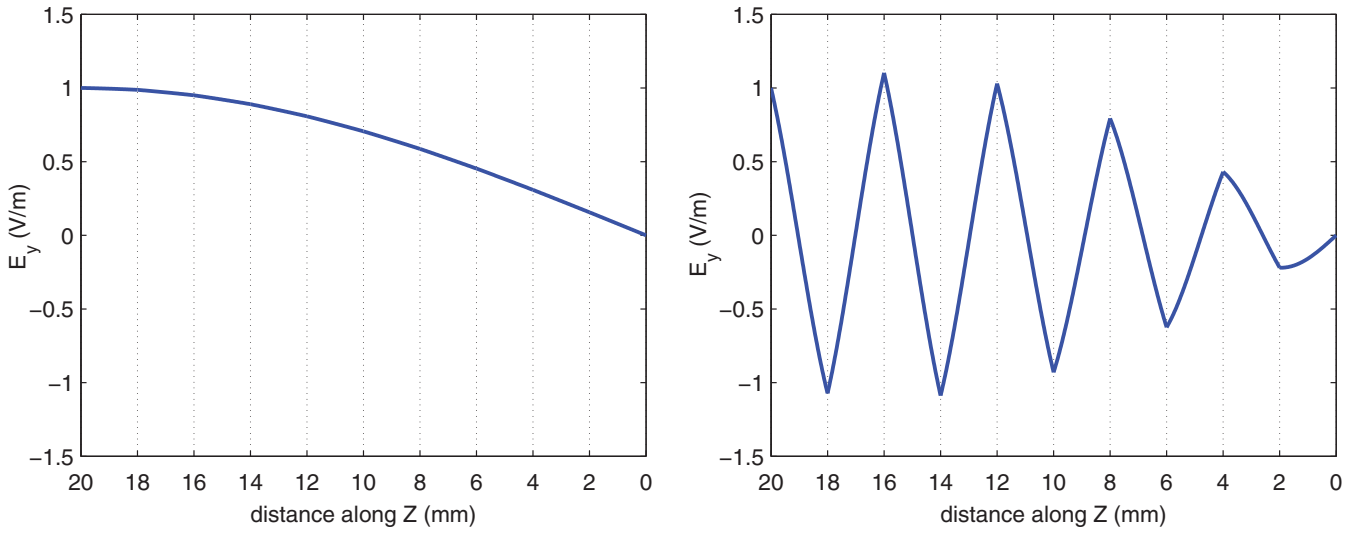

FIG. 14. (Color online) Analytical results of the field distributions in the ten-layer HIS patch absorber for (a) first resonance mode and (b) last resonance mode.

consequence of this behavior is that the first resonance can be tuned to very low frequencies, with the overall thickness of the structure still being electrically small. This is not possible when meshes are used. Also, it is interesting to see that the field distribution for the first resonance in the patch-loaded slabs is extremely smooth [shown in Fig. 14(a)] when compared with the ripples appearing in the similar plot for the mesh-loaded slabs [shown in Fig. 11(a)]. This difference in the field behaviors could be attributed to the fact that the perturbation introduced by the patches is much stronger than the perturbation introduced by the meshes. The electric-field distributions corresponding to the first and last resonance modes of the ten-layer structure are shown in Fig. 14. The analytical results shown in the figure are the averaged fields per period of the patch array (macroscopic fields). It is observed that these resonance modes have the same qualitative behavior for any number of layers. The field distribution corresponding to the first resonance mode is nearly a quarter-wavelength in the entire multilayer configuration. Also, it is seen that this field distribution is of the same qualitative nature associated with the first resonance of the ten-layer structure without the internal patch grids, i.e., the first mode is largely independent of the patch grids. For the last resonance mode, the field distribution in each layer (except for the last two layers) is nearly a half-wavelength with the electric field crossing the null at the middle of the layer, as shown in Fig. 14(b). This resonance

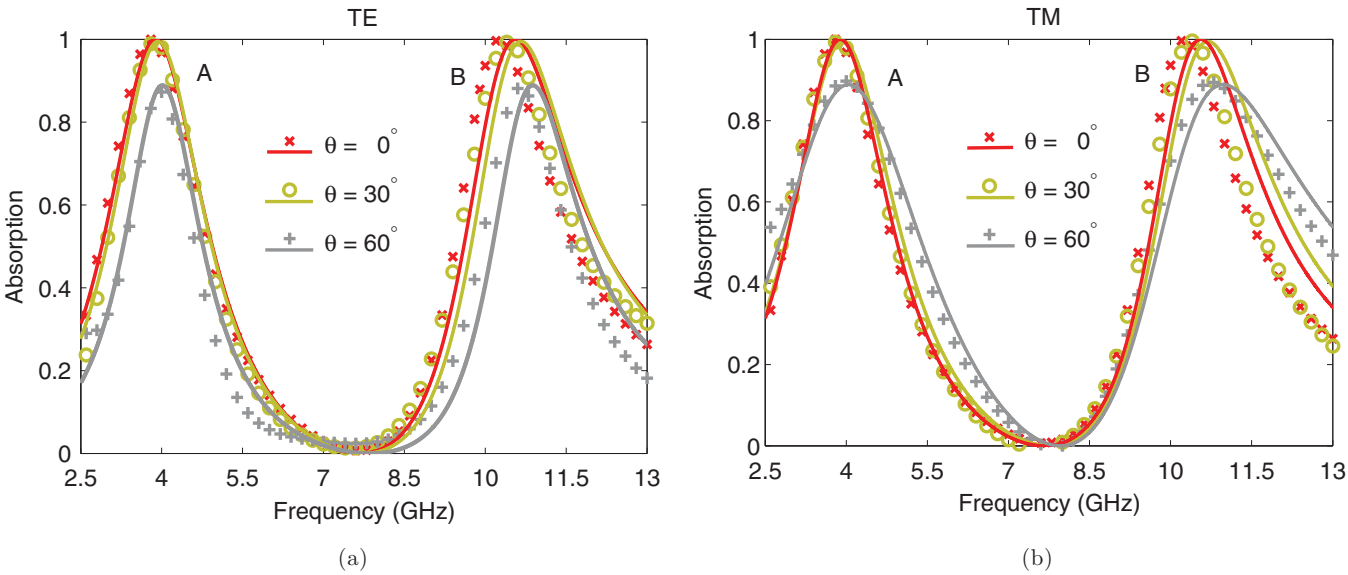

FIG. 15. (Color online) Comparison of analytical (solid lines) and full-wave HFSS results (crosses, circles, and plus signs) of absorption for the two-layer patch array HIS absorber at oblique angles of incidence θ, for (a) TE polarization and (b) TM polarization.

is understood as the FP resonance associated with the single cavity (reactively loaded dielectric slab), and is dependent on the choice of the dielectric and patch grid parameters.

B. Oblique incidence

Now we consider the absorption characteristics of the two-layer HIS patch absorber (with the same dimensions used in the previous example) for oblique angles of incidence and different polarizations. The analytical results predict two absorption peaks as shown in Fig. 15. It can be observed that there is no significant change in the resonance frequencies of the two absorption peaks with the increase in the incidence angle for both polarizations. The reason for the stable resonances can be attributed to the choice of a patch array printed on an electrically thin high-permittivity substrate, as reported in Ref. 14. The explanation offered in Ref. 36 for an angle-independent response could also be used here because the normal polarizability in this structure is negligible in comparison with the tangential polarizability of the patches. However, the surface admittance of the absorber is not perfectly matched to free space at oblique incident angles, thus reducing absorptivity. The values of the absorptivity and resonance frequencies with respect to the incidence angle for both polarizations are given in Table III. It should be noted that the two-layer mesh grid absorber studied in Sec. III A is electrically thick, and because of the choice of a low dielectric constant, it was observed that it is sensitive to the angle and polarization of the impinging plane wave (these results were omitted for the sake of brevity). The alternative explanation given in Ref. 36 is also valid in this case. Total absorption peaks for different polarizations of obliquely incident plane waves can be achieved by employing a tunable resistive sheet. The idea here is to adjust the admittance of the resistive sheet (Y_R) in accordance to the admittance of free space for oblique incident angles of TE- and TM-polarized plane waves [given in Eq. (2)]. For instance, to achieve the unity absorption peaks, the resistive sheet of the two-layer absorber is adjusted to the value of $1/188.5$ S for the case of a TM-polarized plane wave incident at 60^{o}. Specifically, we have calculated the reflected electric-field distributions for the two resonance modes (with the resonance frequencies of 4.03 and 10.96 GHz) of the absorber, and the full-wave simulations are shown in Fig. 16. It can be observed that there is no reflected field in the air region (above the resistive sheet) and the field is confined to the absorber.

TABLE III. Absorptivity ($\mathcal{A}$) as a function of the incident angle and polarization.

θ (deg)	Mode A (GHz)	Mode B (GHz)	$\mathcal{A}$
TE 0	3.88	10.55	1
TE 30	3.93	10.66	0.99
TE 60	4.01	10.88	0.88
TM 0	3.88	10.55	1
TM 30	3.93	10.69	0.99
TM 60	4.03	10.96	0.88

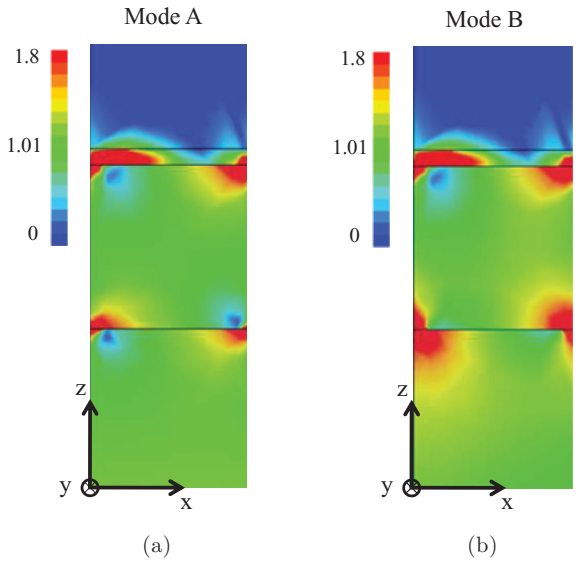

FIG. 16. (Color online) HFSS results of the reflected field distributions of a two-layer HIS patch absorber for the case of a TM-polarized plane wave incident at 60°: (a) first resonance mode and (b) second resonance mode.

V. CONCLUSION

In this work, a simple circuit model has been applied to the analysis of the absorption properties of multilayer structures with subwavelength dimensions in the microwave regime. The results obtained by this method are in complete agreement with the numerical simulations. It is observed that at low frequencies, the resonances of complete absorption occur, and it is shown that these resonances are of FP type corresponding to the strongly coupled individual reactively loaded dielectric slabs. The observed resonances have been characterized by studying the electromagnetic field behavior using the circuit model and numerical simulations. For the case of a fishnet absorber, it has been noticed that the number of peaks in the absorption band is equal to the number of dielectric slabs, and all the peaks are within a characteristic frequency band. The lower and upper band edges of the absorption band are explained in terms of the series of strongly coupled FP cavities, and it is shown that these band edges are largely independent of the overall length of the structure.

In addition, we show that a two-layer absorber formed by printing patch arrays on an electrically thin high-permittivity substrate is insensitive to the angle and the polarization of the impinging plane wave. Also, it is shown that total absorption for oblique incidence can be achieved by using a tunable resistive sheet.

ACKNOWLEDGMENTS

This work has been partially supported by the Spanish Ministerio of Science and Innovation and European Union FEDER funds (projects TEC2010-16948 and Consolider Ingenio 2010 CSD2008-00066) and by the Spanish Junta de Andalucia (Project TIC-4595).

[1]B. A. Munk, *Frequency Selective Surfaces: Theory and Design* (Wiley, New York, NY, 2000).
[2]N. I. Landy, S. Sajuyigbe, J. J. Mock, D. R. Smith, and W. J. Padilla, Phys. Rev. Lett. **100**, 207402 (2008).
[3]B. Wang, T. Koschny, and C. M. Soukoulis, Phys. Rev. B **80**, 033108 (2009).
[4]N. I. Landy, C. M. Bingham, T. Tyler, N. Jokerst, D. R. Smith, and W. J. Padilla, Phys. Rev. B **79**, 125104 (2009).
[5]H. Tao, C. M. Bingham, A. C. Strikwerda, D. Pilon, D. Shrekenhamer, N. I. Landy, K. Fan, X. Zhang, W. J. Padilla, and R. D. Averitt, Phys. Rev. B **78**, 241103 (2008).
[6]X. Liu, T. Starr, A. F. Starr, and W. J. Padilla, Phys. Rev. Lett. **104**, 207403 (2010).
[7]Y. Avitzour, Y. A. Urzhumov, and G. Shvets, Phys. Rev. B **79**, 045131 (2009).
[8]J. Hao, J. Wang, X. Liu, W. J. Padilla, L. Zhou, and M. Qiu, Appl. Phys. Lett. **96**, 251104 (2010).
[9]F. Bilotti, A. Toscano, K. B. Alici, E. Ozbay, and L. Vegni, IEEE Trans. Electromag. Compat. **53**, 63 (2011).
[10]N. Engheta, Proc. IEEE **2**, 392 (2002).
[11]S. Simms and V. Fusco, Electron. Lett. **41**, 1311 (2005).
[12]H. Mosallaei and K. Sarabandi, Proc. IEEE **1B**, 615 (2005).
[13]Q. Gao, Y. Yin, D.-B. Yan, and N.-C. Yuan, Microw. Opt. Technol. Lett. **47**, 228 (2005).
[14]O. Luukkonen, F. Costa, C. R. Simovski, A. Monorchio, and S. A. Tretyakov, IEEE Trans. Antennas Propag. **57**, 3119 (2009).
[15]D. J. Kern and D. H. Werner, Microw. Opt. Technol. Lett. **48**, 2468 (2002).
[16]F. Costa, A. Monorchio, and G. Manara, IEEE Trans. Antennas Propag. **58**, 1551 (2010).
[17]Q. L. Zhou, C. L. Zhang, K. J. Mu, B. Jin, L. L. Zhang, W. W. Li, and R. S. Feng, Appl. Phys. Lett. **92**, 101106 (2008).
[18]L. Cugunov, A. Mednis, and J. Kliava, J. Phys. Condens. Matter **3**, 8017 (1991).
[19]H. Tao, C. M. Bingham, D. Pilon, K. Fan, A. C. Strikwerda, D. Shrekenhamer, W. J. Padilla, X. Zhang, and R. D. Averitt, J. Phys. D **43**, 225102 (2010).
[20]Q. Y. Wen, H. W. Zhang, Y. S. Xie, Q. H. Yang, and Y. L. Liu, Appl. Phys. Lett. **95**, 241111 (2009).
[21]J. Brown, Proc. IEE, pt. 4 **100**, 51 (1953).
[22]W. Rotman, IRE Trans. Antennas Propag. **10**, 82 (1962).
[23]S. A. Tretyakov and S. I. Maslovski, Microw. Opt. Technol. Lett. **38**, 175 (2003).
[24]Y. Q. Li, Y. Q. Fu, and N. -C. Yuan, Microw. Opt. Technol. Lett. **51**, 1775 (2009).
[25]R. Ulrich, Infrared Phys. **7**, 37 (1967).
[26]R. Sauleau, Ph. Coquet, J. P. Daniel, T. Matsui, and N. Hirose, Int. J. Infrared Millimeter Waves **19**, 1693 (1998).
[27]C. S. R. Kaipa, A. B. Yakovlev, F. Medina, F. Mesa, C. A. M. Butler, and A. P. Hibbins, Opt. Express **18**, 13309 (2010).
[28]N. Engheta, A. Salandrino, and A. Alu, Phys. Rev. Lett. **95**, 095504 (2005).
[29]S. Tretyakov, *Analytical Modeling in Applied Electromagnetics* (Artech House, Boston, MA, 2003).
[30]O. Luukkonen, C. Simovski, G. Granet, G. Goussetis, D. Lioubtchenko, A. V. Raisanen, and S. A. Tretyakov, IEEE Trans. Antennas Propag. **56**, 1624 (2008).
[31]HFSS: High Frequency Structure Simulator based on the Finite Element Method, Ansoft Corporation [http://www.ansoft.com].
[32]D. F. Sievenpiper, L. Zhang, R. F. J. Broas, N. G. Alexopoulos, and E. Yablonovich, IEEE Trans. Microwave Theory Tech. **47**, 2059 (1999).
[33]W. McKinzie and S. Rogers, Proc. IEEE **2**, 423 (2003).
[34]C. R. Simovski, P. de Maagt, and I. V. Melchakova, IEEE Trans. Antennas Propag. **53**, 908 (2005).
[35]C. Fabry and A. Perot, Ann. Chim. Phys. **16**, 115 (1899).
[36]J. A. Gordon, C. L. Holloway, and A. Dienstfrey, IEEE Antennas Wireless Propag. Lett. **8**, 1127 (2009).